Journal of Sound and Vibration 455 (2019) 324–338

Contents lists available at ScienceDirect

Journal of Sound and Vibration

journal homepage: www.elsevier.com/locate/jsvi

Noise reduction inside a cavity coupled to a flexible plate with embedded 2-D acoustic black holes

Hongli Ji [a, b, 1], Xiaodong Wang [a, 1], Jinhao Qiu [a, *], Li Cheng [b, *], Yipeng Wu [a], Chao Zhang [a]

[a] State Key Laboratory of Mechanics and Control of Mechanical Structures, Nanjing University of Aeronautics and Astronautics, Nanjing, China

[b] Department of Mechanical Engineering, Hong Kong Polytechnic University, Hung Hom, Kowloon, Hong Kong

ARTICLE INFO

Article history:
Received 13 December 2018
Received in revised form 29 March 2019
Accepted 2 May 2019
Available online 16 May 2019
Handling Editor: D. Juve

Keywords:
Vibro-acoustic properties
Cavity noise
Acoustic black hole
Coupling analysis

ABSTRACT

Acoustic black hole (ABH) structures have been exploited to manipulate the flexural wave propagation with results showing a great potential for structural vibration damping enhancement and suppression of free-field acoustic noise radiation. In the present paper, ABHs are used to reduce the noise inside a cavity bounded by a flexible plate with multiple two-dimensional (2-D) ABH indentations. The interior sound field is generated by and fully coupled to the vibration of the flexible plate subject to a point force excitation. A refined numerical finite element model considering the plate-cavity coupling is established and validated by experiments. Both the simulation and experimental results show a significant noise reduction inside the cavity in a relatively wide frequency range through embedding the 2-D ABHs into the flexible plate. Analyses on the underlying mechanisms show a dual physical process of the ABH effects: the first being the direct consequence of the vibration reduction of the plate as a result of ABH-induced damping enhancement, whilst the second one being caused by a reduction in the coupling strength between the plate and the cavity. This ABH-specific decoupling phenomenon is characterized by the spatial coupling coefficients, which depend on the degree of morphological matching between structural modes and acoustic modes over the plate-cavity interface. The reported phenomenon of the impaired structural-acoustic coupling reveals a new ABH-specific feature which enriches the existing knowledge on ABH structures.

1. Introduction

The vibro-acoustic system, comprising a hard-walled enclosure and a light flexible plate, has received a great deal of attentions in the past half-century, due to its academic significance and wide engineering applications, for instance, car compartments, aircraft cabin and space capsule, etc. [1–3]. The problem is challenging because of the complex nature of the coupling between the structural vibration and the acoustic field, as evidenced by the fact that the mere suppression of the

* Corresponding authors.
E-mail addresses: qiu@nuaa.edu.cn (J. Qiu), li.cheng@polyu.edu.hk (L. Cheng).

[1] These authors contributed equally to this work and should be considered co-first authors.

https://doi.org/10.1016/j.jsv.2019.05.004
0022-460X/

structural vibration may not systematically lead to a reduction in the interior sound of the enclosed space. Therefore, the consideration of vibro-acoustic coupling is necessary [4].

Research on acoustic black holes (ABHs) has been attracting a growing attention in the last decade [5–10]. The ABH phenomenon, an acoustic analogy of astrophysical black hole, takes advantages of the propagation properties of the structure-borne flexural waves in thin-walled structures. By properly tailoring the structural thickness and adopting suitable damping treatment, flexural waves are focalized and dissipated, conducive to structural vibration suppression. More specifically, when the thickness of a one-dimensional ABH beam satisfies a power-law variation $h(x) = \varepsilon x^m$, $(m \geq 2)$, the phase velocity of the flexural wave decreases to zero as it approaches the taper edge, thus annulling wave reflection theoretically. For a two dimensional plate, the thickness of the structure can also be tailored (to power-law-profiled indentations or pits) to produce similar phenomena, forming a type of lens which focuses the structure-borne energy to a specific location. An attractive feature of the ABHs is the possibility of being embedded into the structure to achieve the design of lighter structures. The resulting high energy concentration is conducive to various applications such as passive vibration control, energy harvesting, and free-field sound radiation control.

Alongside the ever-increasing interests, a wide range of studies have been carried out, focusing on different aspects of ABH structures. Existing works range from fundamental studies on the modeling [11,12], analytical and experimental analyses [9,13,14], phenomenon characterization [9,11–15] and applications [14,16–19]. Up to now, most of researches predominantly focus on vibration control, but less on noise reduction. In the latter category, a representative work is the one on acoustic performance of a plate containing six ABHs [20], with results showing an obvious reduction of sound radiation into a free space. Sound radiation from a plate embedded with a grid of ABH indentation was also studied to show that an ABH-featured plate reduces the low-frequency sound radiation [21]. Besides, a wavenumber transform analysis was also carried out to investigate the structural acoustic coupling of the ABH system and determine the radiation efficiency of the embedded ABHs plate compared to a uniform plate [22]. The ABH-induced transonic boundary changes and supersonic acoustic intensity analyses also confirmed the creation of subsonic waves in a plate [23]. However, all these studies focused on free-field problems. To our best knowledge, no studies have been reported on application of ABH structures for cavity noise control. The problem is different from the free-field radiation problem in terms of physics because of the structure-acoustic coupling. There is a need to investigate the issue and to gain physical insights into the underlying mechanisms of ABH-specific features under a fully coupled vibro-acoustic context.

The goal of this paper is twofold: to investigate and show the potential of using ABH structures for the interior sound reduction; and to explore and understand the underlying physics and noise reduction mechanisms. To this end, a typical configuration consisting of an acoustic cavity bounded by an elastic plate with multiple embedded ABH indentations is investigated. The paper is organized as follows. The system under investigation and the experimental setup used are first introduced in section 2. In section 3, numerical analysis method and performance evaluation indicators are described. A finite element model considering the full cavity-plate coupling is established. The model is refined using experimental data and further used to compute both the vibration of the plate and the acoustic field inside the cavity based on the modal superposition approach. The sound field inside the cavity with an ABH-plate is analyzed both experimentally and numerically, in comparison with that of a uniform plate in section 4. In section 5, the mechanism behind the observed cavity noise reduction by ABH structures is further explained from the ABH-induced changes in the plate vibration, its sound radiation efficiency and the coupling between the ABH-plate and the acoustic cavity. Conclusions are drawn in section 6.

2. Description of the system and experimental setup

The system considered in this study is shown in Fig. 1. A cuboid cavity with a dimension of $0.6 \times 0.4 \times 0.36$m and made of plexiglass of 0.04 m thick, is covered by an elastic plate on the top. These plexiglass panels are fairly massive so that the walls can be considered as acoustically rigid. The elastic plate was made of steel, which was clamped to the edges of the cavity as rigidly as possible by using two steel frames and twenty-four bolts. All the junctions were well sealed using rubber to avoid possible gaps and sound leakage. For comparison, two types of elastic plates, one with four 2-D ABH indentations (called ABH-plate) and the other without ABHs (called uniform plate) were investigated. Both the ABH-plate and the uniform plate have the same dimension of 0.6×0.4m with a thickness of 0.0052 m. The width of the clamped area at each edge is 0.04 m. Since the ideal ABH profile was difficult to fabricate due to limited machining precision, a modified 2-D ABH profile proposed by Huang et al. was used [15]. The four identical ABH indentations were machined on one side of the ABH-plate by CNC milling, which are equally spaced along the diagonal of the plate, as shown in Fig. 2(a). Referencing to the coordinate system in Fig. 2, the centers of the four ABH indentations are (0.13, 0.1), (0.13, −0.1), (−0.13, −0.1), and (−0.13, 0.1), respectively. Each ABH indentation consists of a tapered region and a plateau with a constant thickness at its center, as shown in Fig. 2(b), whose thickness profile is described as:

$$h(r) = \begin{cases} 0.0002, & (r \leq 0.01) \\ 1.389(r - 0.01)^2 + 0.0002, & (0.01 \leq r \leq 0.07) \end{cases} \tag{1}$$

where r is the radial distance from the center of each ABH indentation. A circular butyl rubber constrained damping layers with a thickness of 0.002 m and a diameter of 0.035 m was bonded to the central area of each ABH indentation. Material parameters of the plate and those of the damping layers are tabulated in Table 1.

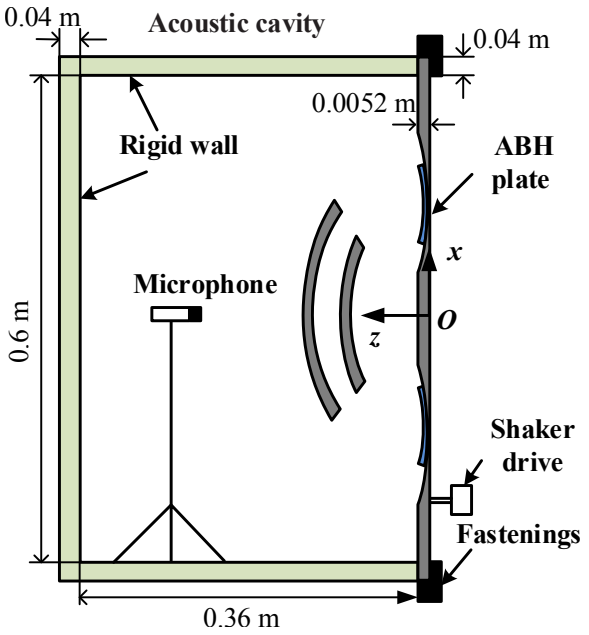

Fig. 1. The configuration of the vibro-acoustic cavity system.

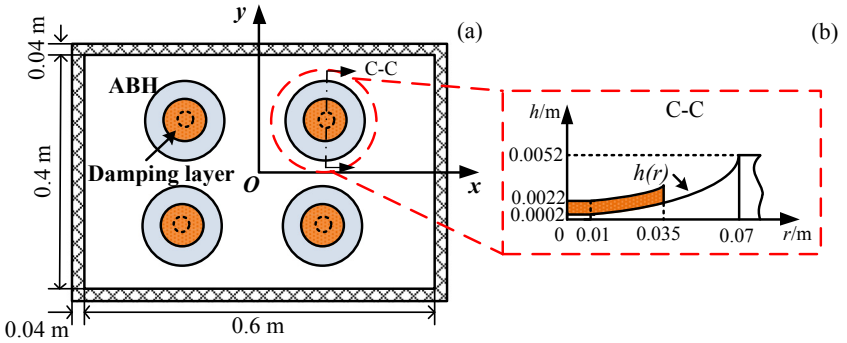

Fig. 2. Plate with modified 2-D ABHs.

Table 1
Material properties of the plate and the damping layer.

Plate	Damping layer
$E_p = 206$ GPa	$E_d = 0.1$ GPa
$\rho_p = 7850$ kg/m^3	$\rho_d = 1780$ kg/m^3
$\nu_p = 0.28$	$\nu_d = 0.45$
$\eta_p = 0.004$	$\eta_d = 0.28$

In the experiment, a white noise (100–5000 Hz), generated by a signal generator and amplified by a power amplifier (YMC LA-200) was used to drive an electromagnetic shaker (YMC VT-50) to excite the flexible plate at (−0.24, −0.025, 0), as shown in Fig. 3. A flexible slim rod was used to connect the shaker and the plate through a force transducer (PCB 208C02) to measure the excitation force. The vibration velocity of the plate was measured by a Polytec Laser Scanning Vibrometer (PSV 500) at two points, L_1 (0, −0.1, 0) and L_2 (0.065, 0.05, 0). Two microphones, located at M_1 (−0.05, 0.1, −0.2052) and M_2 (0.05, −0.03, −0.2052), respectively, were used to measure the acoustic pressure inside the cavity. Measured analog signals were acquired through an A/D converter (NI 9234) for further processing.

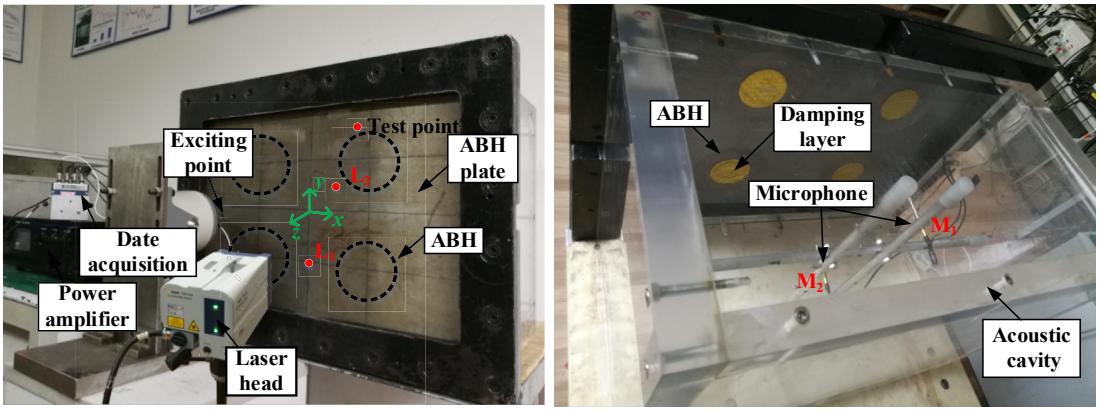

Fig. 3. Experimental test set-up.

3. Simulation method and FEM model

A FEM model is developed based on the three-dimensional elastic theory in conjunction with the acoustic field description. For the benefit of readers, analysis principles and the definition of some evaluation indicators to be used in the subsequent analyses are briefed.

3.1. Coupling analysis and evaluation indicators

The discretized vibro-acoustic coupling equation of the plate-cavity system can be expressed in the following general form:

$$\begin{bmatrix} M_s & 0 \\ -\rho_0 C & M_a \end{bmatrix} \begin{Bmatrix} \ddot{w} \\ \ddot{p} \end{Bmatrix} + \begin{bmatrix} D_s & 0 \\ 0 & D_a \end{bmatrix} \begin{Bmatrix} \dot{w} \\ \dot{p} \end{Bmatrix} + \begin{bmatrix} K_s & C^T \\ 0 & K_a \end{bmatrix} \begin{Bmatrix} w \\ p \end{Bmatrix} = \begin{Bmatrix} B \\ 0 \end{Bmatrix} F \tag{2}$$

where w is the vector of nodal displacement of the plate; $p$the vector of nodal sound pressure inside the cavity; ρ_0 the density of air; M, D and K the mass, damping and stiffness matrices for the structure and acoustic field, respectively. C is a matrix representing the coupling between the plate and the acoustic field; F the excitation force and B a vector related to nodal force.

Based on the conventional modal superposition theory, $w$and $p$can be decomposed over the *in-vacuum* structural mode shape functions $\varphi = \{\varphi_1, \cdots, \varphi_{n_s}\}^T$ and the rigid-walled acoustic mode shape functions $\psi = \{\psi_1, \cdots, \psi_{n_a}\}^T$, respectively, as

$$w = \varphi q_s \tag{3}$$

$$p = \psi q_a \tag{4}$$

where q_s and q_a are the modal coordinates of the plate and cavity, respectively. It should be noted that the viscoelastic damping layer was considered in the structural modeling, but the damping effects were ignored in the modal analysis so that all the structural modes are real. Using the orthogonality property of shape functions and considering the effect of viscous damping, Eq. (2) can be cast into the following form:

$$\begin{bmatrix} \overline{M}_s & 0 \\ -\rho_0 \overline{C} & \overline{M}_a \end{bmatrix} \begin{Bmatrix} \ddot{q}_s \\ \ddot{q}_a \end{Bmatrix} \begin{bmatrix} \overline{D}_s & 0 \\ 0 & \overline{D}_a \end{bmatrix} \begin{Bmatrix} \dot{q}_s \\ \dot{q}_a \end{Bmatrix} + \begin{bmatrix} \overline{K}_s & \overline{C}^T \\ 0 & \overline{K}_a \end{bmatrix} \begin{Bmatrix} q_s \\ q_a \end{Bmatrix} = \begin{Bmatrix} \varphi^T & B \\ 0 \end{Bmatrix} F \tag{5}$$

where $\overline{C} = \psi^T C \varphi$ is the coupling matrix between the structural modes and acoustic modes; $\overline{M}_s$, $\overline{D}_s$, and $\overline{K}_s$ are diagonal matrices of structural modal mass, damping and stiffness, respectively and $\overline{M}_a$, $\overline{D}_a$, and $\overline{K}_a$ are their acoustic counterparts. Equation (5) is the vibro-acoustic coupling equation of the system in the modal space. Based on above formulation, the responses of vibration and acoustic field of the structure-cavity coupling problem under a given excitation can be solved with the help of commercial finite element code ABAQUS and VIRTUAL.LAB.

For analysis, four indices are defined for characterizing system damping, cavity noise reduction, efficiency of sound radiation by the plate into the cavity and the coupling property between the structural and acoustic modes, respectively.

The mean quadratic velocity of the plate is defined to evaluate the vibration level of the plate as:

$$Lv_e = 10\log\frac{\left\langle \overline{v_n^2} \right\rangle}{v_{ref}^2} \tag{6}$$

where

$$\left\langle \overline{v_n^2} \right\rangle = \frac{1}{2S}\int_S v_n v_n^* dS \tag{7}$$

with v_n is the normal velocity of the plate and S the whole vibrating surface.

The space-averaged sound pressure inside the enclosure is used to evaluate the performance of the noise reduction [24]:

$$Lp_e = 10\log\frac{\left\langle \overline{p_e^2} \right\rangle}{p_{\text{ref}}^2} \tag{8}$$

where

$$\left\langle \overline{p_e^2} \right\rangle = \frac{1}{2V}\int_V pp^* dV \tag{9}$$

with V and p being the volume and the acoustic pressure, respectively.

The radiation efficiency is an important parameter to evaluate the noise radiation capability of a vibrating structure into a free space. However, its traditional definition has no clear physical meaning for cavity problems due to appearance of standing waves inside the cavity. Instead, the cavity radiation efficiency is defined as:

$$\overline{\sigma} = 10\log\frac{E_s}{\rho_0 V\overline{\langle v_n^2 \rangle}\Big/2} \tag{10}$$

where E_s is the total acoustic energy inside the cavity, expressed as:

$$E_s = \frac{1}{4}\int \rho_0 v_a v_a^* dV + \frac{1}{4}\int \frac{pp^*}{\rho_0 c_0^2} dV \tag{11}$$

In which v_a is the acoustic velocity of the air particles inside the cavity.

For the ease of analysis, a modal coupling coefficient is defined as

$$\overline{C}_{ij} = \frac{1}{S}\psi_i^T C\varphi_j = \frac{1}{S}\int_S \widehat{\psi}_i \widehat{\varphi}_j dxdy \tag{12}$$

where the modal vectors $\widehat{\psi}_i$, which only contains the pressure at the interface, is the reduced form of the ith acoustic mode in the cavity, ψ_i, and the modal vectors $\widehat{\varphi}_j$, which only includes the normal displacement at the interface, is the reduced form of the jth vibration of mode, φ_j. It should be noted that the same symbols have been used for both modal functions in the physical space and modal vectors in discretized space in the above expressions.

Details and discussions on the relationship among these performance indices and the system parameters are given in Appendix. In the most rigorous sense, the local viscoelastic coating should result in complex modes so that the phase of vibration of a given mode varies with position, thus leading to a complex coupling coefficient. Calculations were conducted to verify the differences between the modulus of the complex coupling coefficients with the ones calculated using real modes presented above. Results show that the discrepancies between both are acceptably small for the present configuration.

3.2. The FEM model refinement

A FE model was first developed with a view to reveal the physical phenomena on one hand, and to be further used to explore the underlying physical mechanism on the other hand. Based on the three-dimensional equation of motion, the plate was discretized using C3D20 solid elements in ABAQUS, which is a second-order element with 20 nodes. The considered frequency range in analysis was from 100 Hz to 5000 Hz. Coarse meshes were used in the area outside the ABH indentations and finer meshes were used in the central area of the ABHs to ensure more than ten elements per local wavelength at twice

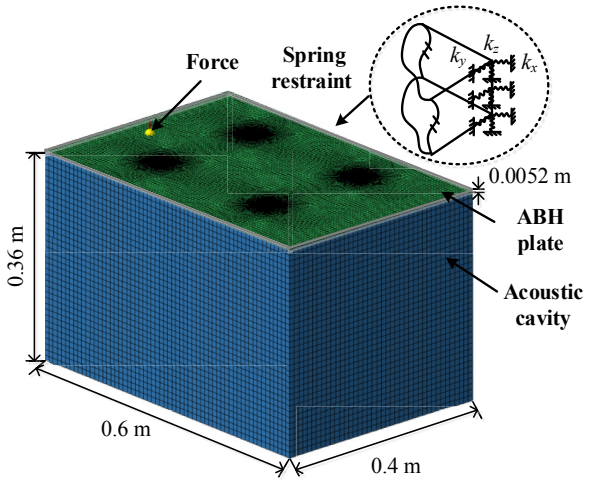

Fig. 4. The FE model of vibro-acoustic cavity system.

the maximum frequency of interest, as shown in Fig. 4. The total number of elements for the ABH-plate is 32424. The damping layer and the metal part of the plate were connected by common node technique. The uniform plate, used for comparison purposes, was also meshed using a non-uniform grid.

A uniform mesh grid was used for acoustic analysis of the cavity. To guarantee the computation accuracy, at least six elements per local wavelength at twice the maximum frequency of interest were used. Cubic acoustic elements with sides of 10 mm were used. The interaction between the plate and the acoustic field was realized by a coupling surface, which established data mapping without the need of matching between the structural mesh of the plate and the cavity mesh for acoustic field.

A harmonic excitation force with an amplitude of 1 N was applied to the plate. Modal loss factors of the acoustic cavity modes were assigned as 0.001. The damping of the plate was more complicated due to the losses in the clamped boundaries so that a model refinement is necessary in numerical analysis to take the effect of the imperfect boundary conditions into consideration. In this study, the clamped boundaries of the plate were modeled by assigning proper spring constants to the boundary nodes of the FEM model, as shown in Fig. 4 k_x, k_y and k_z are specific stiffness constants of the two distributed in-plane spring and the distributed out-of-plane spring, respectively, defined in unit area of the cross-section. It was assumed that k_x are k_y are the same along the same edge, and k_x, k_y and k_z take the same set of values for the two opposite sides of the four boundaries. The damping effect of the boundaries was apprehended by modifying the damping model of the plate which is a combination of the Rayleigh damping and the structural damping. The former is defined by two coefficients α and β, which are the proportionality constants of the mass matrix and stiffness matrix, respectively [25], and the latter by a complex elastic modulus. The structural damping coefficient was set to a nominal value of 0.004, as shown in Table 1, while the coefficients α and β were to be identified using experimental data. The specific stiffness constants of the boundaries were estimated by minimizing the difference between the numerical and experimental results of the natural frequencies of the first six modes and the coefficients α and β were estimated by minimizing the difference between the numerical and experimental value of modal damping ratio of the first six modes. The estimated value of coefficients α and β are 11.2 and 3.82×10^{-7}, respectively, in this study.

3.3. Validations of the numerical model

The experimentally measured natural frequencies and damping ratios of the first six modes of the ABH-plate and the corresponding numerical results from the refined numerical model are listed in Table 2. Errors of the natural frequency of the

Table 2
The first six modal frequencies and damping ratios of ABH-plate.

Modal number	Modal frequencies (Hz)		Damping ratio	
	FEM	Experiment	FEM	Experiment
1	138.2	141.2	0.0079	0.0083
2	230.5	231.3	0.0055	0.0056
3	351.4	338.1	0. 0042	0.0042
4	361.0	358.5	0.0040	0.0040
5	453.1	451.5	0.0036	0.0035
6	530.3	538.8	0.0033	0.0031

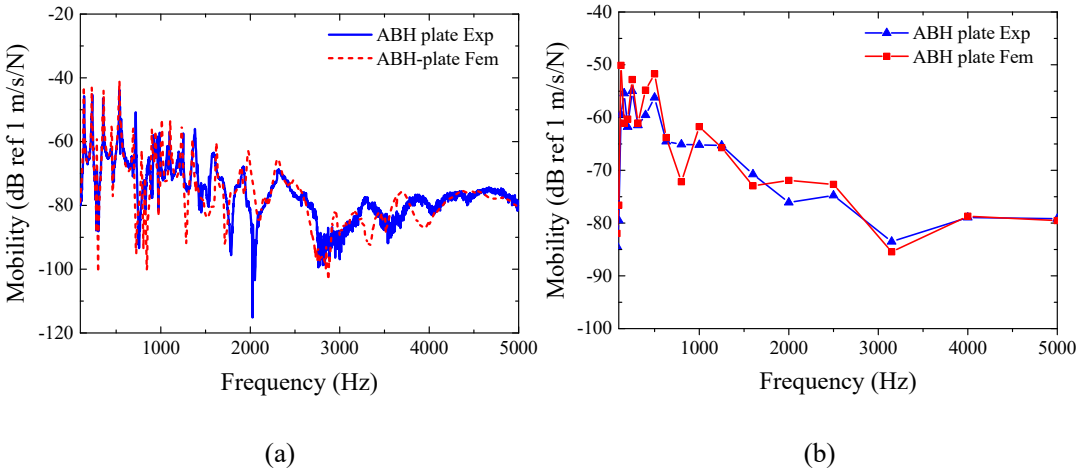

Fig. 5. Comparison between the experiment and simulation results of cross point mobility at L_2: (a) and (b) are ABH-plate in narrow band and one-third octave bands.

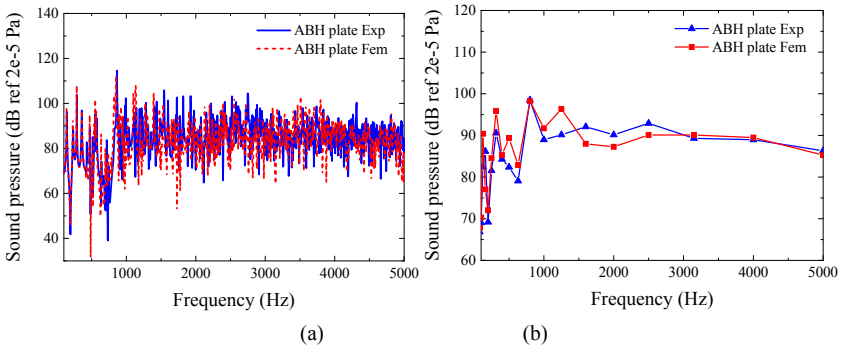

Fig. 6. Comparison between the experiment and simulation results of sound pressure level at M_2: (a) and (b) are ABH-plate in narrow band and one-third octave bands.

first six modes are less than 4%. Since the acoustic field is only coupled with the dominant bending modes of the plate, all the modes dominated by in-plane displacements are neglected in the simulation. The number of structural modes considered in the simulation for the frequency range of interest is $n_s = 140$ for the ABH-plate and $n_s = 93$ for the uniform plate. Fig. 5(a) shows the comparison between the numerical and experimental results in terms of the mobility of the ABH-plate at L_2. It can be seen that the numerical results from the refined model are in good agreement with the experimental ones despite some differences at some particular frequencies, which is further confirmed by the corresponding one-third octave plot in Fig. 5(b). The experimental and numerical results of cross point mobility at L_2 for the uniform plate also agree well with each other (not shown here).

As to the acoustic response, the sound pressure at M_2 in the cavity with an ABH-plate are shown in Fig. 6(a) and (b), in which experimental and numerical results are also compared. Apart from the structural mode-induced peaks, additional ones due to the acoustic resonances in the cavity are clearly seen. The number of the acoustic modes used in the simulation is $n_a = 1368$. Since the cavity resonance is three-dimensional, there are much more acoustic modes than structural modes and more resonance peaks in the frequency response in Fig. 6(a) than in Fig. 5(a). These results explain how the cavity noise differs from free-field radiation and why cavity noise reduction is more difficult. Once again, numerical results from the refined model can be considered to be in good agreement with the experimental ones. Considering the complex cavity-plate configuration and its rich dynamics, it can be concluded that the developed numerical model satisfactorily characterizes the physical system and can be further used as a reliable tool for system analyses.

4. ABH-induced cavity noise reduction

The performance of cavity noise reduction by the ABH-plate is first investigated both experimentally and numerically and compared with its uniform counterpart.

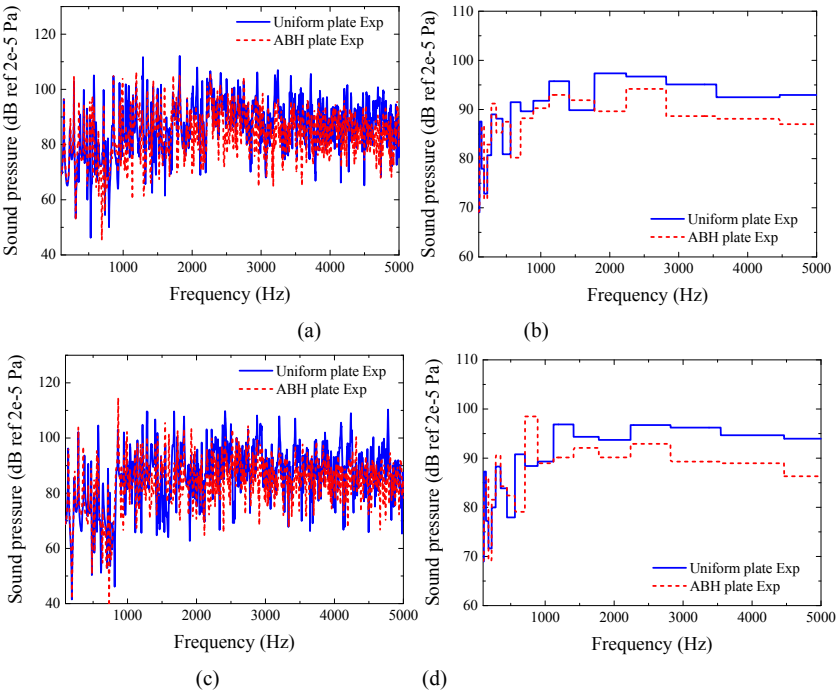

Fig. 7. Experimental results of sound pressure level in narrowband and one-third octave bands: (a) and (b) at M_1; (c) and (d) at M_2.

Fig. 7(a) and (c) show the spectra of the sound pressure measured at M_1 and M_2 inside the cavity of the ABH-plate and the uniform plate, respectively. Results indicate that the sound pressure in the cavity of the ABH-plate is reduced in a wide frequency range, compared with the case of uniform plate. The reduction is more obvious and systematic in the higher frequency range where the ABHs are apparently more effective. The mean sound pressure in the one-third octave bands for both plates are also shown in Fig. 7(b) and (d), further confirming the benefit of the ABH structure in terms of the noise reduction inside the cavity.

To better reflect the global noise reduction performance, the space-averaged sound pressure is calculated with result shown in Fig. 8. Obviously the first acoustic mode at 284 Hz and the fourth acoustic mode at 510 Hz, which are not strongly observable at M_1 and M_2, are strongly excited in the cavity. Furthermore, it can be seen from Fig. 8(a), the overall trend of space-averaged sound pressure is consistent in the low frequency range below 1300 Hz, although the sound pressure slightly increases at some frequencies and decreases at others. Significant noise reduction occurs mainly at frequencies above 1300 Hz. From 1300 Hz to 2100 Hz, Fig. 8(c) shows a sound pressure decrease of 5–20 dB, especially at most resonant frequencies. At higher frequencies (above 2100 Hz), the sound pressure is reduced throughout the entire frequency band.

The mean sound pressure in one-third octave bands shown in Fig. 8(b) gives a more global description on the noise reduction performance evaluation. It can be seen from Fig. 8(b) that the reduction in the space-averaged sound pressure in the cavity with the ABH-plate, albeit slightly lower, is very similar to the experimental results in Fig. 7(b) and (d). Nevertheless, a space-averaged sound level reduction, ranging from 3 to 10 dB, can be observed in the frequency above 1300 Hz. However, no obvious reduction can be observed in the frequency range below 1300 Hz.

Above numerical and experimental results reveal the benefit of embedding ABH indentations for interior noise reduction purposes. Although this is coincidentally similar to the observations made in the free field, the underlying physics and mechanisms might be different due to the drastic differences of the two types of problems. In free-field sound radiation or transmission problems, the reduced sound radiation is attributed to the ABH-induced reduction in the structural wave velocity, thus creating acoustically slow structural waves which are less efficient in sound radiation into the far field [21–23]. In the present cavity case, near-field effect dominates the structural-acoustic coupling. Therefore, it is surmised that the observed interior sound reduction may involve a different physical mechanism. This is to be discussed in the following using the developed FE model.

5. Control mechanisms and discussions

In order to understand the observed ABH-induced noise reduction mechanism, analyses are conducted to examine the damping characteristics, radiation efficiency and the coupling coefficient defined in Section 3.1. Eq. (A.12) shows that the

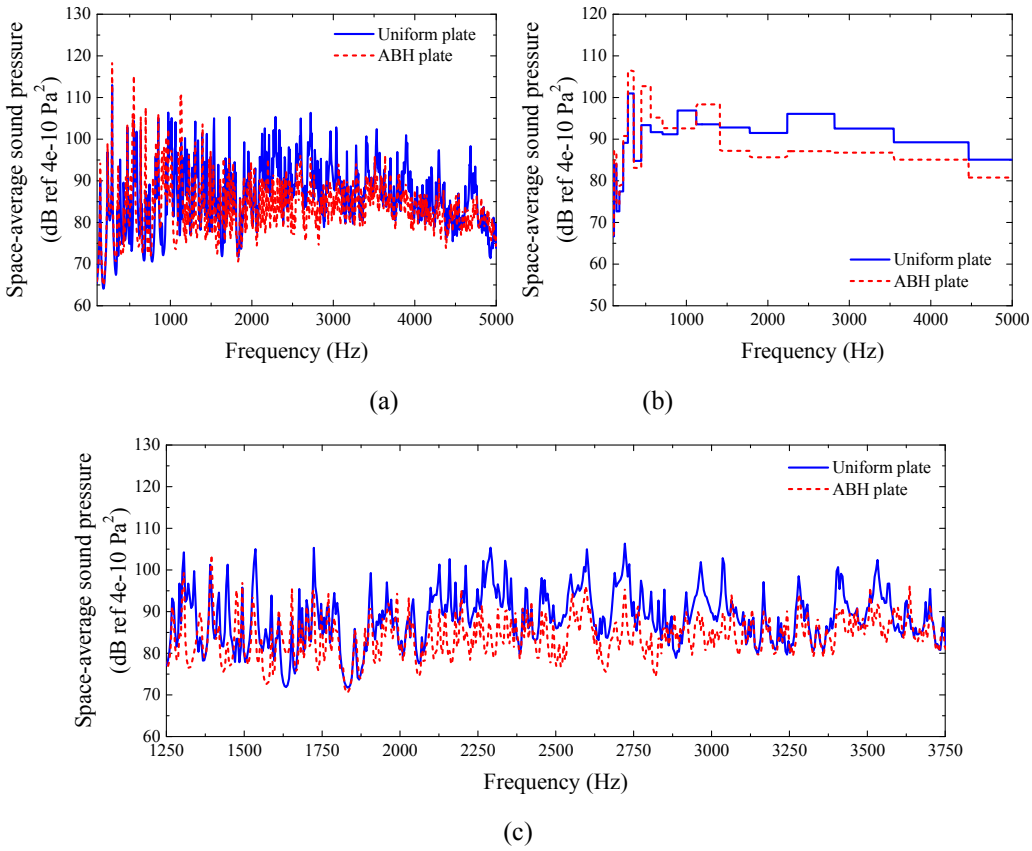

Fig. 8. Space-averaged sound pressure level of the cavity: (a) narrow band; (b) one-third octave bands; (c) narrow band from 1250 Hz to 3750 Hz.

space-averaged sound pressure is directly determined by the mean quadratic velocity and the radiation efficiency and Eqs. (A.9-A.11) indicate that the radiation efficiency depends on the coupling coefficient.

5.1. *Mean quadratic velocity, radiation efficiency and coupling coefficient*

The simulation results of the surface mean quadratic velocity and the modal loss factors of both the ABH-plate and the corresponding uniform plate are shown in Figs. 9 and 10, respectively. It can be seen that, while the responses of both plates being very similar below 1300 Hz, vibration attenuation in the ABH-plate is obvious compared with the uniform plate above 2500 Hz. Between 1300 Hz and 2500 Hz, however, the ABHs show their effectiveness in vibration attenuation at most frequencies. Previous studies on ABH structures [21] showed that one of the important parameters to characterize the ABH effects is the so-called characteristic frequency f_c, at which the wavelength of the free bending wave in a uniform plate equals the diameter of ABHs, defined as follows:

$$\left[\frac{f_c \times (D_{\mathrm{ABH}})}{c}\right] = 1.0 \tag{13}$$

where c is the velocity of the bending wave in the uniform plate,D_{ABH} is the diameter of ABHs. In the present case, f_c is 2567 Hz. Above the characteristic frequency (high frequency range), structural modes are dominated by local deformation within the ABH indentation and their modal loss factors are significantly increased as compared with the uniform plate (Fig. 10).

Apparently, ABH effects are cut on somewhere between 1300 Hz and 2500 Hz, which is below the characteristic frequency. In this frequency band, there exist both local resonance modes and a few global vibration modes in the ABH-plate. The vibration at the local modal frequencies is well suppressed due to ABH-induced damping enhancement. For example, local modes appear at 1479 Hz and 1773 Hz, having a modal loss factors of 0.07611 and 0.04734, respectively. This can be explained by the local resonance phenomenon in the ABH-plate [21,26]. The local resonance modes concentrate the vibration energy in the central area of ABHs so that the energy can be effectively dissipated by the damping layer, which play an important role in vibration damping of ABHs structure. On the contrary, the modes at 1621 Hz and 1699 Hz are global ones (Fig. 9(b)). Therefore,

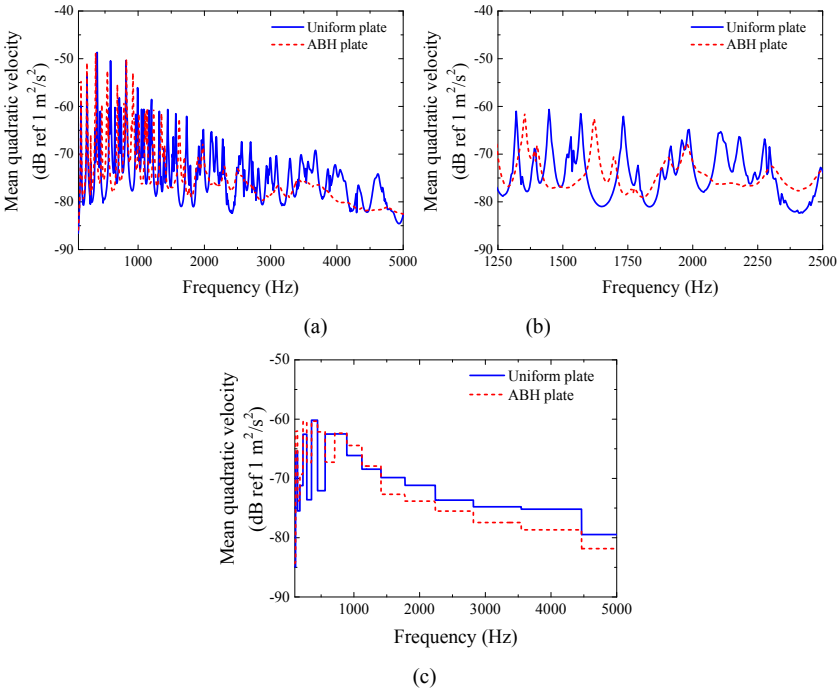

Fig. 9. Mean quadratic velocity of the plate: (a) narrow band; (b) narrow band from 1250 Hz to 2500 Hz; (c) one-third octave bands.

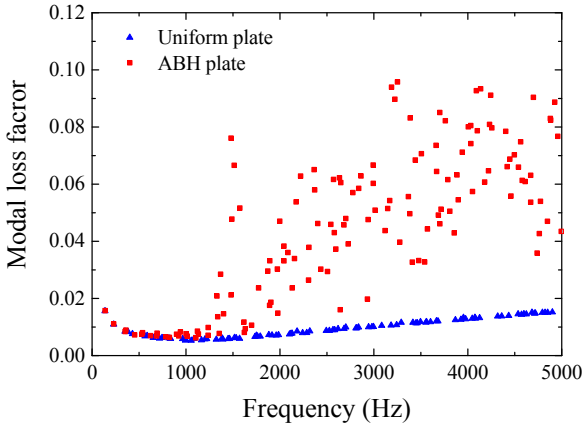

Fig. 10. Modal loss factor of the ABH-plate vs uniform plate.

these two modes are poorly damped, with modal loss factors of 0.00811 and 0.01062, respectively. The first local mode of the ABH-plate appears at 1368 Hz, below which (low frequency range) all the modes are global ones and the modal loss factors of the ABH-plate are almost the same as those of the uniform plate as shown in Fig. 10.

The radiation efficiencies of both plates are shown in Fig. 11, showing different variation trends before and after 1300 Hz. As expected, the radiation efficiency of the ABH-plate is similar with that of the uniform plate below 1300 Hz before local modes appear. Above 1300 Hz, the radiation efficiency of ABH-plate is significantly lower than that of the uniform plate at almost all the resonance peaks. It means that the acoustic energy inside the cavity covered with the ABH-plate is much smaller than that covered with a uniform plate for the same given mean quadratic velocities of plates. Note that nearly all the peaks in Fig. 11(a) are the cavity modal frequencies, since structural modes have been effectively damped out by the ABH effects in this frequency range. Hence, the observed reduction in the radiation efficiency is due to the change of the vibro-acoustic characteristics. The reduction in the one-third octave bands is from 3 to 10 dB above 1300 Hz.

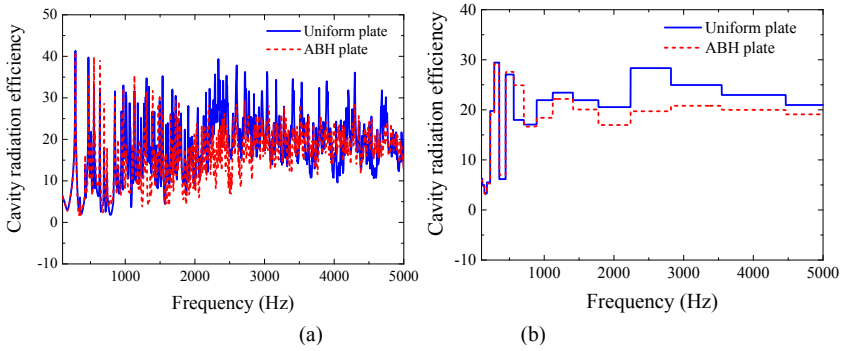

Fig. 11. Cavity radiation efficiency of the plate-cavity system: (a) narrow band; (b) one-third octave bands.

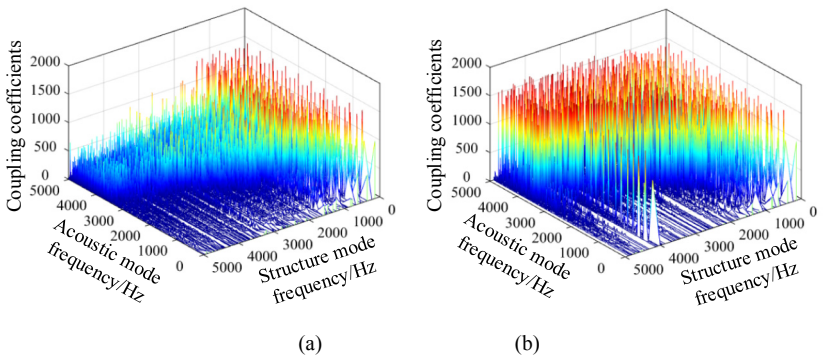

Fig. 12. The coupling coefficients of the structural modes and acoustics modes in the whole frequency range: (a) ABH-plate with 140 structural modes and 1368 acoustic modes; (b) Uniform plate with 93 structural modes and 1368 acoustic modes.

The analysis of the coupling coefficients, based on formulation detailed in the Appendix, can further shed light on this. As shown in Eq. (A.11), the radiation efficiency depends on the coupling coefficients between an acoustic mode and a structural mode. The overall coupling coefficients of the two plate-cavity systems are shown in Fig. 12. It is obvious that the coupling coefficients of ABH-plate-cavity are systematically smaller than those of the uniform-plate-cavity in the high frequency range, but they are almost the same in the low frequency range. As shown by Eq. (12), the coupling coefficients depends on the degree of morphological matching between the structural modal function and acoustic modal function. As an example, examine the acoustic mode at 3038 Hz, which is close to a structural mode at 3119 Hz of the ABH-plate and the mode at 3083 Hz for the uniform plate, respectively. Fig. 13 shows the corresponding acoustic and structural mode shapes at the plate-cavity interface. Since the mode of the ABH-plate at this frequency is a local resonance mode as shown in Fig. 13(b), the degree

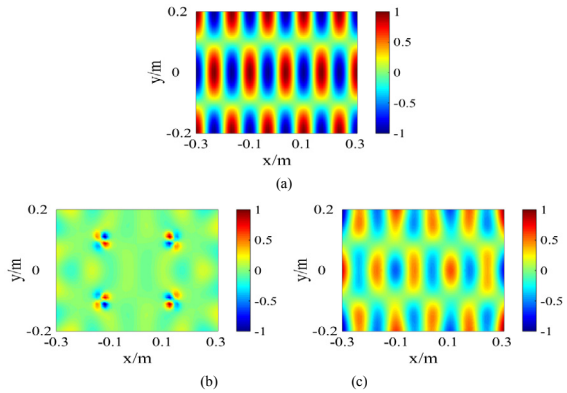

Fig. 13. Mode shapes: (a) Acoustic mode at 3038 Hz; (b) ABH-plate mode at 3119 Hz; (c) Uniform plate mode at 3083 Hz.

Table 3
Comparison of ABH-plate-cavity and uniform plate-cavity.

Acoustic modal frequency	Uniform plate			ABH-plate			Mean quadratic velocity/dB	Cavity radiation efficiency/dB	Space-averaged sound pressure/dB
	Structural modal frequency	Coupling coefficient	Structural modal coordinate	Structural modal frequency	Coupling coefficient	Structural modal coordinate	Uniform/ABH-plate	Uniform/ABH-plate	Uniform/ABH-plate
850 Hz	820 Hz	199.92	1.05E-07	823 Hz	316.99	1.54E-07	−69.94/-68.06	31.56/30.84	105.01/106.15
	836 Hz	278.20	7.57E-08	899 Hz	0.07	1.64E-08			
	965 Hz	0.02	7.96E-09	923 Hz	0.05	4.10E-08			
	2114 Hz	148.48	2.17E-08	2086 Hz	0.08	4.40 E−09	−67.78/-76.25	25.64/23.46	101.31/90.63
2125 Hz	2128 Hz	0.08	5.62 E−08	2131 Hz	157.64	8.92E-09			
	2183 Hz	0.01	1.36 E−08	2155 Hz	0.06	1.14E-10			
	2996 Hz	269.86	1.15 E−08	2994 Hz	65.73	3.19 E−09	−77.62/-78.37	35.55/24.51	101.41/89.60
3038 Hz	3083 Hz	1569.03	7.34E-09	3013 Hz	0.09	5.80 E−09			
	3183 Hz	0.08	6.10 E−10	3119 Hz	474.13	9.18E-09			

of morphological matching between it and the acoustic mode is much lower than that between the structural mode of the uniform-plate and the acoustic mode.

The fact that the structural modes of the ABH-plate are more global in the low frequency range and local in the high frequency range explains why the coupling coefficients of the ABH-plate are almost the same as those of the uniform plate, but start to be significantly smaller in the high frequency range. A further analysis of Eq. (A.9) indicates that only the coupling coefficients between the acoustic modes and the structural modes with close resonance frequencies will contribute to the radiation efficiency.

5.2. The mechanism of noise reduction

According to Eq. (A.13), the reduction of sound pressure inside the cavity are contributed by both the reduction of mean quadratic velocity and the reduction of the radiation efficiency. Although Eq. (A.13) holds for each acoustic resonance frequency, the relationship among the three parameters in one-third octave bands is quite complicated, as shown in Figs. 8, 9 and 11. Furthermore, which factor, the mean quadratic velocity or the radiation efficiency, contributes more should also be discussed. To this end, three typical frequencies of 850 Hz, 2125 Hz and 3038 Hz are considered. The mean quadratic velocity, radiation efficiency and space-averaged sound pressure of the ABH-plate-cavity and uniform plate-cavity at these frequencies are calculated and listed in Table 3. To further shed light on the mechanism of noise reduction, the coupling coefficient of the acoustic resonance of the cavity and the dominant structural modes with close frequencies are also listed in the table. Obviously, Eq. (A.13) holds at these three frequencies according to the data in the last three columns.

At the acoustic mode of 850 Hz the mean quadratic velocity, the space-averaged sound pressure and the radiation efficiency are almost the same for the ABH-plate and uniform plate. It means that all the three terms in Eq. (A.13) are almost zero. This is consistent with the previous analysis.

At 2125 Hz, the mean quadratic velocity, the radiation efficiency and the sound pressure are reduced by about 8.47 dB, 1.18 dB and 10.68 dB, respectively, by replacing the uniform plate with the ABH-plate. Since the radiation efficiency is determined mainly by the coupling coefficient of the dominant structural mode and the acoustic mode, which is 157.64 and 148.48, respectively for the two plates, because there is only one dominant mode. The mean quadratic velocity is determined by the structural modal coordinate. As seen from Table 3, the magnitude of the structural modal coordinate is 8.92E-09 and 2.17E-08 for the ABH-plate and uniform plate, respectively, equivalent to a reduction of about 8 dB. At this frequency, the decrease of the vibration leads to the sound pressure reduction for the ABH-plate-cavity.

At the acoustic mode of 3038 Hz, the mean quadratic velocities are very similar for both the ABH-plate and uniform-plate. Following the same logic and examining the variation level of the coupling coefficients, it can be concluded that the reduction of the cavity noise is mainly due to reduction of the coupling coefficient in this case.

According to the above discussion, it can be concluded that the sound pressure attenuation can be attributed to the reduction of the plate vibration as a result of damping enhancement and a simultaneous reduction of coupling coefficient. While the former attenuates the structure-dominant peak resonance level, the latter allows an overall weakening of the structural-acoustic coupling in the effective ABH range, thus resulting in a systematic reduction of the acoustic responses inside the cavity, including non-resonance frequency regions. Therefore, the obvious advantage of ABHs is their capability to reduce both the resonance vibration of the structure and the structure-acoustic coupling of the system in a wide frequency range.

6. Conclusions

In this study, the potential of ABH structures for interior noise reduction in a plate-cavity system is investigated both experimentally and numerically. The vibro-acoustic cavity system consists of a rigid rectangular acoustic cavity covered with a flexible plate with embedded 2-D ABHs. A refined numerical finite element model considering the plate-cavity coupling was established and validated by experiments. Both experimental and simulation results show the effectiveness of ABH effects on cavity noise reduction. It is shown that above the characteristic frequency, the sound pressure can be effectively reduced by embedding ABHs into the plate. Below the frequency of the first local resonance, however, no systematic noise reduction effect can be observed. In the frequency range between the first local resonance frequency and the characteristic frequency, noise is well reduced at most frequencies, except at several frequencies due to the global mode of the plate. Analyses on the underlying mechanisms show a dual physical process of the ABH effects: the first being the direct consequence of the reduced vibration level of the plate as a result of ABH-induced damping enhancement, whilst the second one being caused by a reduction of the coupling strength between acoustic modes and structural modes. This ABH-specific decoupling phenomenon is characterized by a spatial coupling coefficient, which depends on the degree of morphological matching between a structural mode and an acoustic mode over the plate-cavity interface, which is significantly small between the local resonance modes of the ABH-plates and the acoustic modes. The reported phenomenon of the impaired structural-acoustic coupling reveals a new ABH-specific feature which enriches the existing knowledge on ABH structures.

Acknowledgements

This research was supported by National Natural Science Foundation of China (No. 11532006 & 51775267), Research Grants Council of Hong Kong Special Administrative Region, China (PolyU 152009/15E and PolyU152017/17E), Natural Science Foundation of Jiangsu Province (BK20181286), Aeronautical Science Fund (No. 20161552014), Fundamental Research Funds for the Central Universities (No. NE2015001), the equipment pre-research foundation (No. 61402100103), Six talent peaks project in Jiangsu Province Class C (No. JXQC-002) and A Project Funded by the Priority Academic Program Development of Jiangsu Higher Education Institutions.

Appendix

The dependence of the performance indicators upon the modal coordinates and the relationship between different performance indicators defined in Section 3.1 are clarified. In the numerical analysis, Eq. (5) was solved in the fully coupled form in the FEM code with some approximations. At a specific frequency, the excitation force is expressed as $F = \tilde{F}e^{i\omega t}$, where i is the imaginary unit. The structural modal coordinate is expressed as $q_{sj} = \tilde{q}_{sj}e^{i\omega t}$, where $\tilde{q}_{sj}$ is the complex amplitude of the jth structural mode. Since the coupling term in the structural dynamic equations in Eq. (5) is much smaller than the external excitation, it is assumed that the influence of acoustic pressure in the structural vibration is negligible and $\tilde{q}_{sj}$ is determined solely by the external excitation.

According to Eq. (3), with the reduced structural modal vectors, the normal velocity of the plate can be expressed as:

$$v_n = i\omega\widehat{\varphi}q_s = i\omega\sum_j \tilde{q}_{sj}\widehat{\varphi}_j \tag{A.1}$$

where $\tilde{q}_{sj}$ is the complex amplitude of the structural modal coordinate. The mean quadratic velocity becomes

$$\overline{\langle v_n^2\rangle} = \omega^2\sum_{i,j}\tilde{q}_{si}\tilde{q}_{sj}^*\frac{1}{2S}\int_S \widehat{\varphi}_i\widehat{\varphi}_j dS \tag{A.2}$$

Obviously, the reduced modal vectors $\widehat{\varphi}_j$ do not meet the orthogonality condition. However, approximate orthogonality can be assumed between these reduced modal vectors because the bending vibration is dominant in the present structural configuration. The property of approximate orthogonality among the reduced modal vectors has also been verified numerically in our study. Hence there exists

$$\overline{\langle v_n^2\rangle} \approx \omega^2\sum_j \left|\tilde{q}_{sj}\right|^2\frac{1}{2S}\int_S \widehat{\varphi}_j^2 dS \tag{A.3}$$

It is obvious that when modal function is normalized according to

$$\frac{1}{S}\int_S \hat{\varphi}_j^2 dS = 1 \tag{A.4}$$

The mean quadratic velocity is the summation of all the squared magnitude of the modal coordinate at this frequency.

Next, the acoustic field at the resonance frequency of the ith acoustic mode is considered. Because the damping ratio of the acoustic modes is very small, the influence of the non-resonance modes can be neglected. According to Eq. (4), the acoustic field can be expressed as:

$$p = \tilde{q}_{ai}\psi_i \tag{A.5}$$

where

$$\tilde{q}_{ai} = \frac{e^{-i\pi/2}}{2\zeta_{ai}}\frac{\tilde{F}_{ai}}{K_{ai}} \tag{A.6}$$

Is the complex amplitude of the acoustic modal coordinates,$\tilde{F}_{ai}$ is modal force, K_{ai} is the modal stiffness and ζ_{ai} is the damping ratio of the ith acoustic mode. According Eq. (5), the modal force can be expressed as

$$\tilde{F}_{ai} = -\rho_0\omega_{ai}^2 S\sum \overline{C}_{ij}\tilde{q}_{sj} \tag{A.7}$$

Substituting Eq. (A.7) into Eq. (A.5) and then into Eq. (9) gives the space-averaged sound pressure at the ith acoustic mode in the following form:

$$\overline{\langle p_e^2\rangle} = \frac{\rho_0^2\omega_{ai}^4 S^2}{4\zeta_{ai}^2 K_{ai}^2}\left|\sum_j \overline{C}_{ij}\tilde{q}_{sj}\right|^2 \frac{1}{2V}\int_V \psi_i^2(x,y,z)dV \tag{A.8}$$

Though the above equation includes the contribution from all the structural modes, the magnitude of $\tilde{q}_{sj}$ is very small when the difference between ω_{sj} and ω_{ai} is great enough. In practice, only a few structural modes, whose natural frequency ω_{sj} are very close to ω_{ai}, have to be considered. The above result also indicates that the coupling coefficient $\overline{C}_{ij}$ is very important to evaluate the contribution of a structural mode to an acoustic mode. This also suggests that the contribution of a given mode to the space-averaged sound pressure at the resonance frequency of a given acoustic mode can be effectively reduced by reducing the coupling coefficient between them.

Further discussion about the radiation efficiency defined in Eq. (10) is also necessary. Since the potential energy and the kinetic energy in Eq. (11) are almost the same, the term in the logarithmic function in Eq. (10) is

$$\begin{aligned}\frac{E_s}{\rho_0 V\overline{\langle v_n^2\rangle}\Big/2} &\approx \frac{V\overline{\langle p_e^2\rangle}\Big/\rho_0 c_0^2}{\rho_0 V\overline{\langle v_n^2\rangle}\Big/2} = \frac{\overline{\langle p_e^2\rangle}}{\rho_0^2 c_0^2\overline{\langle v_n^2\rangle}\Big/2}\\ &= \frac{\omega_{ai}^2 S^2}{2\zeta_{ai}^2 c_0^2}\cdot\frac{\left|\sum_j \overline{C}_{ij}\tilde{q}_{sj}\right|}{K_{ai}^2}\cdot\frac{\frac{1}{V}\int_V \psi_i^2(x,y,z)dV}{\sum_j\left|\tilde{q}_{sj}\right|^2\frac{1}{S}\int_S \hat{\varphi}_j^2 dS}\end{aligned} \tag{A.9}$$

The above expression indicates that the radiation efficiency is the synthetic effect of different structural modes even at the resonance frequency of a specific acoustic mode.

In order to clarify the underlying mechanism, we consider a special case in which the ith acoustic mode is solely induced by the jth structural mode. In this case the above equation is simplified to

$$\frac{E_s}{\rho_0 V\overline{\langle v_n^2\rangle}\Big/2} \approx \frac{\omega_{ai}^2 S^2}{2\zeta_{ai}^2 c_0^2}\cdot\frac{\overline{C}_{ij}^2}{K_{ai}^2}\cdot\frac{\frac{1}{V}\int_V \psi_i^2(x,y,z)dV}{\frac{1}{S}\int_S \hat{\varphi}_j^2 dS} \tag{A.10}$$

If the structural mode vectors have been normalized according to Eq. (A.4) and acoustic modes are normalized according to $K_{ai} = 1$, then the above equation is further simplified to

$$\frac{E_s}{\rho_0 S d\overline{\langle v_n^2\rangle}\Big/2} \approx \overline{C}_{ij}^2 \frac{\omega_{ai}^2 S^2}{2\zeta_{ai}^2 c_0^2} \cdot \frac{1}{V}\int_V \psi_i^2(x,y,z)dV. \tag{A.11}$$

The above expression indicates that the radiation efficiency is directly determined by the coupling coefficient in this special case. The assumption of the special case is applicable to the cases in which one structural mode is dominant with respect to a specific acoustic mode. Therefore, the coupling coefficient takes an important role in cavity noise reduction.

From Eqs. (9) and (A.9), the following relationship can be obtained:

$$\overline{\langle p_e^2\rangle} \approx \frac{\rho_0^2 c_0^2}{2}\overline{\langle v_n^2\rangle} \cdot 10^{\frac{\bar{\sigma}}{10}} \tag{A.12}$$

It indicates that the space-averaged sound pressure is directly determined by the mean quadratic velocity and the radiation efficiency.

If ΔLp_e, ΔLv_e and $\Delta\bar{\sigma}$ are used to express the differences in the space-averaged sound pressure, mean quadratic velocity and radiation efficiency between the ABH-plate system and the uniform plate system, then according to Eq. (A.12), there exists

$$\Delta Lp_e \approx \Delta Lv_e + \Delta\bar{\sigma} \tag{A.13}$$

at each acoustic resonance frequency. If there is only one dominant structural mode, then ΔLv_e is determined by the modal coordinate of the mode and $\Delta\bar{\sigma}$ is determined by the coupling coefficient between the structural mode and the acoustic mode.

References

[1] E.H. Dowell, H.M. Voss, The effect of a cavity on panel vibration, AIAA J. 1 (2) (1963) 476–477.
[2] E.H. Dowell, G.F. Gorman, D.A. Smith, Acoustoelasticity: general theory, acoustic natural modes and forced response to sinusoidal excitation, including comparisons with experiment, J. Sound Vib. 52 (4) (1977) 519–542.
[3] Y.Y. Li, L. Cheng, Vibro-acoustic analysis of a rectangular-like cavity with a tilted wall, Appl. Acoust. 68 (7) (2007) 739–751.
[4] M.C. Junger, D. Feit, Sound, Structures, and Their Interaction, MIT press, Cambridge, 1986.
[5] V.V. Krylov, New type of vibration dampers utilising the effect of acoustic 'black holes, Acta. Acust United Ac. 90 (5) (2004) 830–837.
[6] V.V. Krylov, R. Winward, Experimental investigation of the acoustic black hole effect for flexural waves in tapered plates, J. Sound Vib. 300 (1) (2007) 43–49.
[7] V.B. Georgiev, J. Cuenca, M. Moleron Bermudez, F. Gautier, L. Simon, V.V. Krylov, Numerical and experimental investigation of the acoustic black hole effect for vibration damping in beams and elliptical plates, in: Proceedings of the European Conference on Noise Control, 2009. Edingburgh, UK.
[8] V.V. Krylov, Acoustic black holes: recent developments in the theory and applications, IEEE Trans. Ultrason. Ferroelectr. Freq. Control 61 (8) (2014) 1296–1306.
[9] L. Tang, L. Cheng, H. Ji, J. Qiu, Characterization of acoustic black hole effect using a one-dimensional fully-coupled and wavelet-decomposed semi-analytical model, J. Sound Vib. 374 (2016) 172–184.
[10] S.C. Conlon, P.A. Feurtado, Progressive phase trends in plates with embedded acoustic black holes, J. Acoust. Soc. Am. 143 (2) (2018) 921–930.
[11] V.V. Krylov, Geometrical-acoustics approach to the description of localized vibrational modes of an elastic solid wedge, American Institute of physics 35 (2) (1990) 137–140.
[12] V. Georgiev, J. Cuenca, F. Gautier, L. Simon, V. Krylov, Damping of structural vibrations in beams and elliptical plates using the acoustic black hole effect, J. Sound Vib. 330 (11) (2011) 2497–2508.
[13] V. Denis, F. Gautier, A. Pelat, J. Poittevin, Measurement and modelling of the reflection coefficient of an Acoustic Black Hole termination, J. Sound Vib. 349 (2015) 67–79.
[14] H. Ji, J. Luo, J. Qiu, L. Cheng, Investigations on flexural wave propagation and attenuation in a modified one-dimensional acoustic black hole using a laser excitation technique, Mech. Syst. Sign. 104 (2018) 19–35.
[15] W. Huang, H. Ji, J. Qiu, L. Cheng, Wave energy focalization in a plate with imperfect two-dimensional acoustic black hole indentation, J. Vib Aoust. 138 (6) (2016), 061004.
[16] V. Kralovic, V.V. Krylov, Damping of flexural vibrations in tapered rods of power-law profile: experimental studies, Proceeding of the Institute of Acoustics 29 (Pt 5) (2007) 66–73.
[17] J.J. Bayod, Application of elastic wedge for vibration damping of turbine blade, Journal of System Design and Dynamics 5 (5) (2011) 1167–1175.
[18] E. Bowyer, V.V. Krylov, Experimental investigation of damping flexural vibrations in glass fibre composite plates containing one-and two-dimensional acoustic black holes, Compos. Struct. 107 (2014) 406–415.
[19] E.P. Bowyer, V.V. Krylov, Damping of flexural vibrations in turbofan blades using the acoustic black hole effect, Appl. Acoust. 76 (1) (2014) 359–365.
[20] E.P. Bowyer, V.V. Krylov, Experimental study of sound radiation by plates containing circular indentations of power-law profile, Appl. Acoust. 88 (2015) 30–37.
[21] S.C. Conlon, J.B. Fahnline, F. Semperlotti, Numerical analysis of the vibroacoustic properties of plates with embedded grids of acoustic black holes, J. Acoust. Soc. Am. 137 (1) (2015) 447–457.
[22] P.A. Feurtado, S.C. Conlon, Wavenumber transform analysis for acoustic black hole design, J. Acoust. Soc. Am. 140 (1) (2016) 718–727.
[23] L. Ma, L. Cheng, Sound radiation and transonic boundaries of a plate with an acoustic black hole, J. Acoust. Soc. Am. 145 (1) (2019) 164–172.
[24] L. Cheng, J. Nicolas, Radiation of sound into a cylindrical enclosure from a point-driven end plate with general boundary conditions, J. Acoust. Soc. Am. 91 (3) (1992) 1504–1513.
[25] R.W. Clough, J. Penzien, Dynamics of Structures, Computers & Structures, Inc., Berkeley, 2003.
[26] P.A. Feurtado, S.C. Conlon, An experimental investigation of acoustic black hole dynamics at low, mid, and high frequencies, J. Vib. Acoust. 138 (6) (2016), 061002, 061002-6.